FIRE INDUCED DAMAGE IN STRUCTURES AND INFRASTRUCTURE: ANALYSIS, TESTING AND MODELING

A. IBRAHIMBEGOVIC[1*], A. BOULKERTOUS[1], L. DAVENNE[1], M. MUHASILOVIC[2], J. DUHOVNIK[2], AND A. POKRKLIC[3]
[1]*Ecole Normale Supérieure, LMT-Cachan, Civil Engineering, 61 avenue du president Wilson, 94235 Cachan, France*
[2]*Unverisity of Ljubljana, Mechanical Engineering, Slovenia*
[3]*University of Sarajevo, Faculty of Architecture, Bosnia and Herzegovina*

Abstract. In this work we first review the statistical data on large fires in urban areas, presenting a detailed list of causes of fires, the type of damage to structures and infrastructure built of reinforced concrete. We also present the modern experimental approach for studying the fire-resistance of different structural components, along with the role of numerical modeling to provide a more detailed information on quantifying the temperature and heat flux fields. In the last part of this work we provide the refined models for assessment of fire-induced damage in structures built of reinforced concrete, the most frequently used construction material. We show that the refined models of this kind are needed to provide a more thorough explanation of damage and to complete the damage assessment and post-fire evaluations.

Keywords: Fire induced damage, reinforced concrete, structure, infrastructure, fire tests

1. Introduction

The damage of engineering structures and infrastructure due to devastating fire is probably among the most well known natural disasters that the mankind has had to deal with for already more than thousands of years. The most important early risk was widespread use of natural building materials that are quite sensitive

* To whom correspondence should be addressed. e-mail: ai@lmt.ens-cachan.fr

A. Ibrahimbegovic and M. Zlatar (eds.), *Damage Assessment and Reconstruction After War or Natural Disaster*,

to fires (wood, reed, straw), as well as the creation of first large urban zones and increased risks that they represent. Already, at the time of the emperor Neron (64th year B.C.), a large fire broke out in Rome (legend said that Neron himself started it) that in 7 days demolished 10 out of 14 city districts. The fire disasters accelerated with further urbanization and a number of sadly famous disasters have happened throughout the worlds: 'Great Fire' in London (1666), Edinborough (1700), Copenhagen (1728), Stockholm (1750) or Constantinopole (1766). The fire prevention code in urban areas that was proposed and implemented following these disastrous fires (e.g. see ASTM, 1981; Rojtman, 1985), requiring more rigorous rules on construction materials and building space, was partially successful in reducing the number of fires caused by neglect (even though 60% of urban fires are still caused by neglect).

However, these prevention rules are largely insufficient for preventing the fires spread following the natural or man-made disasters, such as earthquakes or explosions. Some known examples of that kind are: the earthquake caused fire in Lisabon (1775) that had about 60,000 victims and the loss of about 85% of the objects; similar post-earthquake fires in San Francisco (1906), or in Tokio and Jokohama (1923); the fire caused by the technical accidents in Fliksboro, England (1974) after pointing of ciklohexane; fire in Mexico City (1984) after the damage on the gas storage; and finally post-accident fire that occurred on the nuclear power plant in Chernobile (1987) which contributed to the more difficult intervention in preventing the leaks of the radioactive particles in the environment. The large fires that occur at war times were numerous, such as fires from last world war in Germany (Hamburg, Drezden) or Japan (Tokio, Jokohama), as well as the wars in Vietnam and Cambodia; and these fires are often as destructive as the military activities. The present day threat of terrorist attacks has further potential of increasing the risk and the damage from accidental fire, with the most recent sadly famous example of the airplane crash into the World Trade Center, which was finally brought down by fire rather than the airplane impact.

Therefore, since we cannot fully control the extreme fire conditions, we focus in this work upon the improvement of the understanding the effects for this kind of disaster and its consequences. Namely, we describe a considerable effort that is spent nowadays to reduce the fire damage by developing and using modern construction materials with enhanced resistance to fire. We also elaborate upon the experimental procedure on testing different structural concepts with respect to fire resistance, along with the numerical procedures for completing the test results in terms of providing the corresponding values of temperature or heat flux distributions. Finally, we also develop numerical models for representing the structural response to fires, which should help provide better damage estimates due to fire for civil engineering structures and infrastructure. We focus herein

upon the most frequently used construction material – the reinforced concrete. The proposed models are quite refined with respect to the usual models used for the same structures under other kind of extreme loading conditions (e.g. earthquake and dead load) and thus require considerable efforts in development, but provide in return much more precise damage estimates. The models presented herein are likely to play important role in constructing the full picture for causes of fire and in providing the complete damage assessment, by running numerical simulations for different fire scenarios.

2. Fire tests and fluid dynamics computations of temperature and heat flux

Fire tests and experimental works, which are carried out currently in routine manner for different construction materials, are often insufficient to decide the fire resistance of structures under heterogeneous temperature and stress fields. Hence, the complementary fire resistance tests are carried out on structure and infrastructure components, trying to enhance understanding of their behavior under sustained devastating fire conditions. No matter how large number of measurements is made in the tests of this kind, one is required in general to supplement those results with the computer aided investigation of the (reactive) fluid flow.

To that end, we will use Computational Fluid Dynamics (CFD) to provide the forecast for movement, propagation of the chemical reaction (during an accidental large-scale fire) and finally important thermodynamic input data on time dependent temperature change and HRR (Heat Release Rate) – flux at the tunnel-cavern or building walls, for further research on resistibility of a RC structures. In this section we present the kind of analysis and typical results that can be obtained for the temperature and flux fields for fires in confined spaces.

We will consider herein the case study of accidental fires in the transformer facilities for the electrical power production (see the photo to the right). We aim at better understanding of the reactive flow phenomena governing the distribution of the gaseous combustion products, which impacts the visibility in first establishing phase of the fire (in such enclosures) and plays decisive parameter that is used in rescuing and protective actions. Further, the influence of heat irradiance that is represented indirectly in the temperature of walls within the cavern, gives the forecast for possible damages in the construction. A thorough understanding of this complex

phenomenon, driven by buoyancy of hot combustion gases in such non-premixed combustion (NPC) can be provided mostly through numerical simulations. Results of the performed study applying the RANS approach for turbulence treatment in the numerically investigated flow in the enclosure of the power-transformer-station show us here the distribution of the temperature-fields and the heat radiation-contours, providing the pertinent information upon thermal loads to be applied on structures.

Several studies of accidental (both pool fires and) fires in enclosures (see Holmstedt et al., 1996; Miles et al., 1999; Wighus, 1994; Fay, 2003; Vidmar and Petelin, 2006), can be consulted for complementary information. The large scale fires are also studied from standpoint of post-event-investigations (see Chow and Kot, 1980; Leitner, 2001; Gabay, 2002) and their negative consequences (Bendelius, 2002), in order to help provide the guidelines of their treatment. Field-model codes that have been tested in CFD-research (see Magnussen and Hjertager, 1976), do report on good capability of these numerical approaches, used in handling the gaseous reacting flows in covered objects. In spite of the first hardware limitations, a decade and half ago, allowing computational domains with few thousands cells (see Kumar and Cox, 1985, 1988), satisfying results were accomplished in attempts of both validating (see Chasse, 1993; Briollay and Chasse, 1994; Kumar and Cox, 1986; Tuovinen, 1994; Kunsch, 2002; McGrattan, 2002) of software tools and aimed CFD-prognoses for particular explored cases of these fluid-flow phenomena (see Beard et al., 1993).

The treating of the turbulent diffusion flames, one of a characteristic of large-scale fires, was incorporated in codes in terms of an extra source term accounting for the effect of buoyancy in turbulent mixing. These developments are carried out and validated for special purpose codes (see Miles, 2006; Magnussen and Hjertager, 1976; Miles and Kumar, 2004) that use the Cartesian mesh only and assume simple one-step chemistry for combustion modeling. The local reaction rate was calculated from a modified version of the eddy break-up mixing model. A comparatively slow mixing of fuel with oxidant (air) is used to control the rate of reaction. Handling both steady and transient flows, treating the turbulence, the RANS models (including variety of boundary conditions and wall functions with modifications for wall roughness) have been compared in latest studies (see Gao et al., 2004). Following up on these studies (see Sanmiguel-Rojas et al., 2007), and trying to investigate transversal prompt-ventilation in the industrial buildings, we performed transient simulation applying k-ε turbulence treatment of large-scale fire in a newly constructed power-transformer unit, where possible accidental scenario was presumed.

In this study the flow phenomena are computed by the Reynolds Averaged Navier–Stokes (RANS) equations, with the turbulence k-ε model (see Britter and Neophytou, 2005), representing the major characteristic of the applied

CFD-investigation-tool of the FLUENT; and handling the buoyancy by applying the Boussinesq approximation. This approach, is not affected by fluctuation of initial conditions, offering more accurate presentation of the time dependent flow – particularly the distribution of the gaseous combustion products (Liu et al., 2004). Since the investigations have shown that the Mach Number was of the order of 0.022, such a flow can be assumed as incompressible (Ferziger and Peric, 2001). Since incompressible, the fluid does not undergo thermal-caused expansion while crossing the reaction front and the reaction makes no impact onto flow-velocity. Further assumption, to have a planar propagation front of combustion in a motionless fluid, leads to the application of the Boussinesq approximation (Baum et al., 1995) without external forces (Vladimirova, 2006). Here, the flow velocity obeys the incompressible Navier–Stokes equation with a temperature-dependent force term.

The change of temperature is described by an advection–reaction–diffusion equation. For this incompressible gaseous reactive flow at low velocity, the governing equations of the combustion-induced flow read:

$$\frac{\partial \overline{v}_j}{\partial x_j} = 0 \tag{1}$$

$$\frac{\partial \overline{v}_i}{\partial t} + \frac{\partial \left(\overline{v}_i \overline{v}_j \right)}{\partial x_j} = -\frac{1}{\rho} \frac{\partial \overline{p}}{\partial x_i} + \frac{1}{\rho} \frac{\partial \overline{\tau}_{ij}}{\partial x_j} - g_i \alpha \Delta \overline{T} \tag{2}$$

$$\frac{\partial \overline{T}}{\partial t} + \frac{\partial \left(\overline{T} \overline{v}_j \right)}{\partial x_j} = \frac{\partial}{\partial x_j} \left(\frac{\lambda}{\rho c_p} \frac{\partial \overline{T}}{\partial x_j} \right) + \frac{1}{z} R\left(T \right) \tag{3}$$

Here $\overline{v}_i$ denotes the average velocity component, $\overline{T}$ the mean local temperature, $\overline{p}$ the pressure, ρ the density, t the time and x_i the space coordinates. The R(T) = ¼ T (1 – T) stands for reaction rate (Vladimirova, 2006) where the reciprocal value of reaction time-scale is represented by z, λ is the thermal conductivity, c_p is the heat capacity at the constant pressure. Temperature T will be used as expression for reaction-progress-variable as well, whose purpose is to distinguished burned, unburned and partially burned state, providing an easy interpretation of flame propagation. The term $-g_i \alpha \Delta \overline{T}$ denotes buoyancy, treated according to the Boussinesq approximation, where $\Delta \overline{T}$ is showing the difference between local and reference temperature. The symbol g denotes the gravity and α is the coefficient of thermal expansion. The model for the stress tensor (Jongen and Gatski, 2000), $\overline{\tau}_{ij}$ is related to the local strain rate:

$$\tau_{ij} = (\tau_{ij})_N + (\tau_{ij})_T \tag{4}$$

where we distinguish between the Newtonian stress $(\tau_{ij})_N = 2\mu\overline{S}_{ij}$ featuring molecular viscosity; and the turbulent Reynolds stress $(\tau_{ij})_T = 2\mu_T\overline{S}_{ij}$, since the stress rate tensor $\overline{S}_{ij}$ is defined as:

$$\overline{S}ij \equiv \frac{1}{2}\left(\frac{\partial v_i}{\partial x_j} + \frac{\partial v_j}{\partial x_i}\right) \tag{5}$$

and the turbulent viscosity:

$$\mu_T = C_\mu \frac{k^2}{\varepsilon} \tag{6}$$

with k the turbulent kinetic energy and ε the dissipation rate of turbulent energy. The applied k-ε model (Leupi, 2005) is a two-equation eddy viscosity model (see Zhang et al., 2002) that uses transport equations for these two variables (see Britter and Woodburn, 1996). One of these equations governs the distribution through the field of k, the local kinetic energy of the fluctuating motion. The other one leads to the energy dissipation rate ε (Malin and Markatos, 1982).

$$\frac{\partial k}{\partial t} - \nabla\cdot\left(C_\mu \frac{k^2}{\varepsilon}\nabla k\right) = C_\mu \frac{k^2}{\varepsilon} P_d - \varepsilon - G_b \tag{7}$$

$$\frac{\partial \varepsilon}{\partial t} - \nabla\cdot\left(C_\varepsilon \frac{k^2}{\varepsilon}\nabla \varepsilon\right) = C_1 k P_d - \frac{\varepsilon}{k}\left(C_3\lambda_v N^2 + C_2\varepsilon\right) \tag{8}$$

The energy term $G_b = \alpha g_i \frac{\mu_t}{Pr_t}\nabla\overline{T}$ is modeling the buoyancy effects, where Pr_t denotes turbulent Prandtl Number (which is of the order of one). The constants are given: C_1=0.126, C_2=1.92, C_μ=0.09, C_ε=0.07.

The applied tool within the CFD-approach (the k-e model) belongs to the state-of-the-art for the turbulence treatment in simulations of the large-scale (accidental) combustion, with no limitation on the shape of the grid. In order to test the grid-independence of computed results, we ran computations with two different grids: one with a grid of 759,646 tetrahedral cells and the other with an unstructured grid of 1,611,723 hexahedral cells – see Fig. 1. The grids were prepared by using the GAMBIT-mesh generator. Both grids were capable of providing sufficient solution accuracy with respect to the computational domain corresponding to the interior the building of power-transformation station, which has the length of 25 m of, the width of 7 m and the height of 8 m.

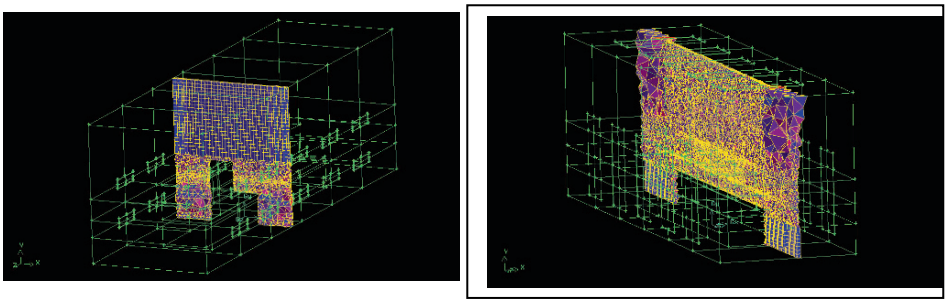

Figure 1. Different grids (with roughly 1,600,000 or 750,000 cells), adapted to the "L-shape" of electric-power-appliance and the interior space of the building of the transformer-unit

For transient simulations (a CFD-mode that was applied in this study (see Brunello et al., 2002) the governing equations must be discretized in both space and time (see Versteeg and Malalasekera, 1995; Sawley and Drotz, 2003). We choose the implicit time-integration and the standard finite volume method (Versteeg and Malalasekera, 1995) for space discretization, along with operator split solution method. The consistent linearization of these equations results in a set of linear equations for each cell in the computational domain, containing the unknown variable at the cell centre as well as the unknown values in surrounding neighbouring cells. In the case when the pressure field and face mass fluxes are not known, FLUENT (Sawley and Drotz, 2003) uses a co-located scheme, where pressure and velocity are both stored at cell centres. The estimation of the boundary conditions in this CFD-based investigation was supported by the experience of some previous studies (Edwards and Hwang, 2005). So were ventilation duct on the roof of the building characterised as open (pressure) boundaries with minor pressure increase or pressure-drop of 10 Pa. The fuel "pool" – the simulated fire-place on the electric-power appliance, was determined by the constant max flux rate of 0.101 kg/m²s having hydraulic diameter of 5.67 m for an approximate 50 MW-heptane fire. The initialisation of computational values for the velocity and pressure was made throughout the whole domain since the global temperature was set to 293 K. The station building walls, were assumed to be adiabatic barriers. This decision was based on some previous research practice. However, a more realistic hypothesis for fire resistance studies of civil-engineering structures would consider the thermal conductivity of walls (e.g. for concrete mixed out of lime-stone sand, we can take $\lambda = 2.3$ W/mK, Gawin et al., 2004) that could provide the appropriate boundary conditions. For our numerical simulations we use wall function boundary conditions in order to avoid a fine meshing in the boundary layer, next to the cavity-walls and we can thus reduce the computational cost. More precisely, the wall shear stress was obtained from the logarithmic law of wall ("wall function") for the distance from the wall, y, the von Karman constant $\kappa = 0.41$ and the constant $C = 9.793$:

$$\frac{\overline{v}}{v_\tau} = \frac{1}{\kappa} ln\, C \frac{v_\tau y}{v} \tag{9}$$

where v_τ denotes the friction velocity, featured within the expression for the wall shear stress:

$$\tau_W = \rho v_\tau^2 \tag{10}$$

The initial conditions of the simulation of this accident, the combustion was assumed to apply to the whole surface that was proclaimed to be fire-source. The numerical solution for the fire-accident in the power-transformer unit is presented in Fig. 2 for the fourth second of this large-scale combustion event. The contours of temperature field show quick fire development with full (negative) impact on the structure.

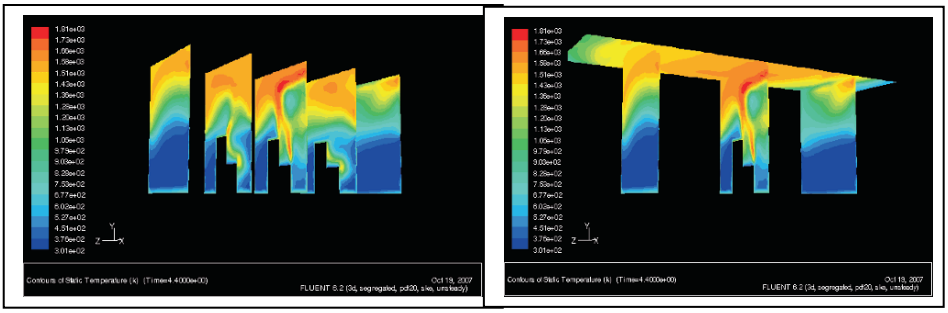

Figure 2. Contours of temperature field in inner space of the power-transformer unit during the simulated accident plotted at several locations within the cavity with typical "mushroom" or "tree-shaped" form of a large-scale pool-combustion; note that the temperature raises over the melting point of the steel in the fourth second of the accidental large-scale fire

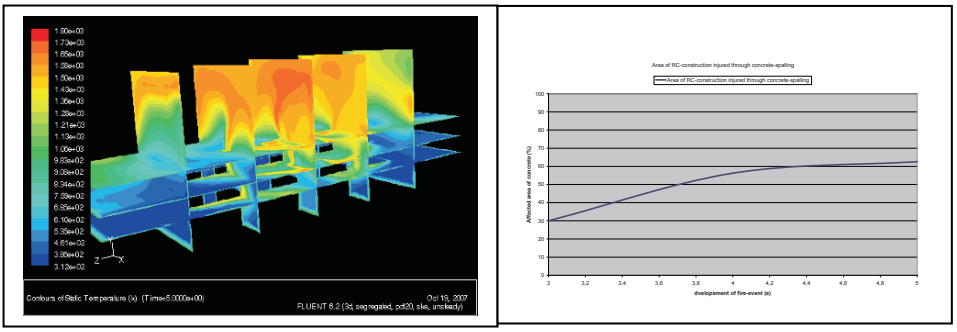

Figure 3. Contours of temperature field in inner space of the power-transformer unit during the simulated accident plotted at several locations within the cavity; note that the temperature raises to the RC spalling temperature in the fifth second of the accidental large-scale fire

For the chosen "fire-size" of this accident is 30 MW as well as a very large volume of inflammable fluid, contained within an electric devices of a power-transformer and switch-unit, contribute to a rather quick fire-spreading accompanying the high thermal power of this confined large-scale accident. The computed results show that after only 5 s (see Fig. 3) of the combustion the temperatures will reach above ~1,100 K (+875°C). The temperatures of this kind can cause a significant damage in structures or infrastructure. In the next section, we review some of the typical damage of most frequently used construction materials.

3. Damage representation due to fire for structures and infrastructure

The reinforced concrete represents the most frequently used construction material for structures and infrastructure. The judicious combination of steel and concrete has provided the best for construction cost, and also the most difficult one to comprehend in terms of its nonlinear inelastic behavior. The most adequate reinforced concrete model depends upon the goal of the present analysis, and the estimate of the damage we would like to obtain. In that respect the choice should be made between: (i) global integrity of the structure built of reinforced concrete under extreme loading, (ii) local integrity of concrete under extreme loading case and (iii) durability of concrete under aggressive environment. The models for each of the listed goals ought to be more and more detailed; see Fig. 4.

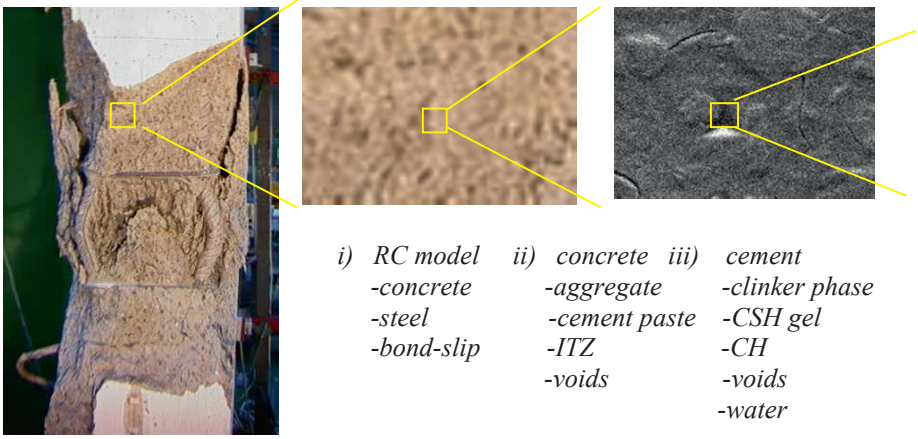

Figure 4. Different models of concrete for computing: (**a**) structure integrity (reinforced-concrete), (**b**) failure criteria (two-phase model of concrete), (**c**) structure durability (multi-phase model of cement)

One of the most dangerous damage mechanisms produced by the large-scale fires, which can especially affect the high-performance concrete, is produced by the spalling phenomena. There exist a couple of competing explanations for spalling (see Bazant and Kaplan, 1996; Ulm et al., 1999; Gawin et al., 2004; Schrefler et al., 2005), illustrated in Fig. 5. The first assumes that the spalling occurs as the joint result of high temperature gradient distribution through the thickness combined with restrained deformation in a massive structure (e.g. tunnel fire, see Tan 2002 and SINTEF 2003), which will jointly produce a compression zone on the surface and the tensile zone in the interior that lead to spalling. The second explanation considers spalling as the results of high temperature gradients accelerating different multi-physics processes, combining thermal (thermal dilatation), chemical (dehydration of cement paste), hydro (evaporation of the liquid pore water, associated by the vapour pressure increase). Accordingly, the main factors that influence spalling are the temperature distribution and its variation inside the concrete element, as well as the characteristics of the considered section (size, shape, permeability, mean pore radius, concrete strength). The vapour pressure can play an important role when a high value is reached during heating, which can produce a kind of explosive spalling, especially in high-density materials like high and ultra high performance concrete.

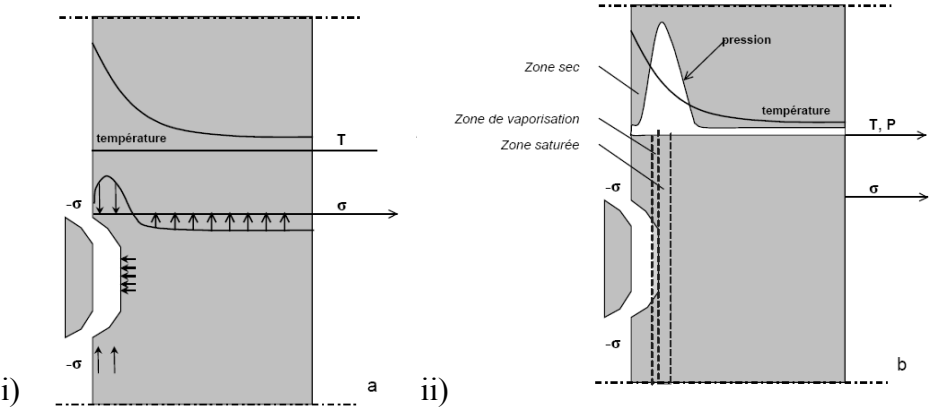

Figure 5. Two different explanations of the spalling phenomena under fire: (**a**) mechanical damage due to high temperature gradient distribution through the thickness, (**b**) pore pressure build-up as a part of hydro-thermo processes under high temperature

The mentioned processes cause an increase of the concrete intrinsic permeability. The joint effect of temperature, gas pressure and material damaging (micro-cracks development) influence the intrinsic material permeability as well. The recent results (see Brunello et al., 2002) indicate that within 5 to 7

min (of fire-combustion only sized as 2.5 MW) inside the concrete walls of a building cavern (at the places differently elevated above the catastrophic fire-place) at the depth of maximum 60 mm from the surface of the concrete, the temperatures of about 700°C are to be noticed – causing the vapour pressure (in the concrete) to reach almost six times higher value than at the ambient, forcing so the kinetics of the thermo-chemical damage.

The spalling phenomena can also be influenced by mechanical damage or cracking of concrete. In fact, it becomes quite important to provide a very reliable representation of the crack spacing and opening in order to evaluate the risk for accelerating the spalling phenomena and the resulting porosity. The key point in that sense is the adequate choice of numerical model for representing the cracks in concrete. The models of this kind will have at least two dissipative mechanisms, the first related to the fracture process zone with a large number of micro cracks and the second related to the localized failure with a large macro crack. Each of mechanisms can be described by a particular plasticity failure criterion (we could also choose the damage criteria). We can thus obtain the basic set of governing equations, which can be written as illustrated in Fig. 6:

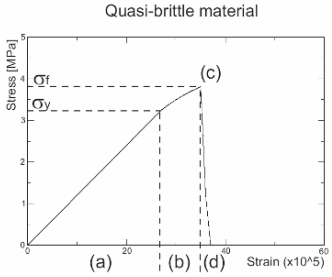

$$
\begin{aligned}
\epsilon &= \epsilon^e + \bar{\epsilon}^p + \bar{\bar{\epsilon}}^p \, \delta x \\
\Psi &\quad (\epsilon^e, \bar{\xi}, \bar{\bar{\xi}}) = \bar{\Psi}(\epsilon^e, \bar{\xi}) + \bar{\bar{\Psi}}(\bar{\bar{\xi}}) \\
\bar{\Phi} &\quad (\sigma, \bar{q}) := |\sigma| - (\sigma_y - \bar{q}) \\
\bar{\bar{\Phi}} &\quad (\sigma, \bar{\bar{q}}) := |t| - (\sigma_f - \bar{\bar{q}}) \\
\dot{\bar{\epsilon}}^p &= \dot{\bar{\gamma}} \frac{\partial \bar{\Phi}}{\partial \sigma} \quad ; \quad \dot{\bar{\xi}} = \dot{\bar{\gamma}} \quad ; \quad \bar{\Phi} \leq 0 \quad ; \quad \dot{\bar{\gamma}} \geq 0 \quad ; \quad \dot{\bar{\gamma}} \bar{\Phi} = 0 \\
\dot{\bar{\bar{\epsilon}}}^p &= \dot{\bar{\bar{\gamma}}} \frac{\partial \bar{\bar{\Phi}}}{\partial \sigma} \quad ; \quad \dot{\bar{\bar{\xi}}} = \dot{\bar{\bar{\gamma}}} \quad ; \quad \bar{\bar{\Phi}} \leq 0 \quad ; \quad \dot{\bar{\bar{\gamma}}} \geq 0 \quad ; \quad \dot{\bar{\bar{\gamma}}} \bar{\bar{\Phi}} = 0
\end{aligned}
$$

Figure 6. 1D representation of failure model for massive structures and governing equations postulating: (i) additive split of total deformation into elastic, smooth plastic and localized plastic field, (ii) strain energy in terms of elastic strain and hardening variables, (iii) plasticity criteria for smooth and localized field, and the evolution equations for the internal variables (note that one over-bar pertains to the FPZ mechanisms, and two bars is used for the internal variables describing the localized failure)

The typical result obtained with models of this kind is given in Fig. 7, for the case of notched specimen under non-proportional loading that starts with tension followed by shear, where we show the spreading of different damage mechanism with contours of micro-cracks and the element-based orientation of macro-cracks. We also show in Fig. 7 the typical sequence of mechanical damage for massive concrete structure, which first starts with micro-cracks followed by macro-cracks.

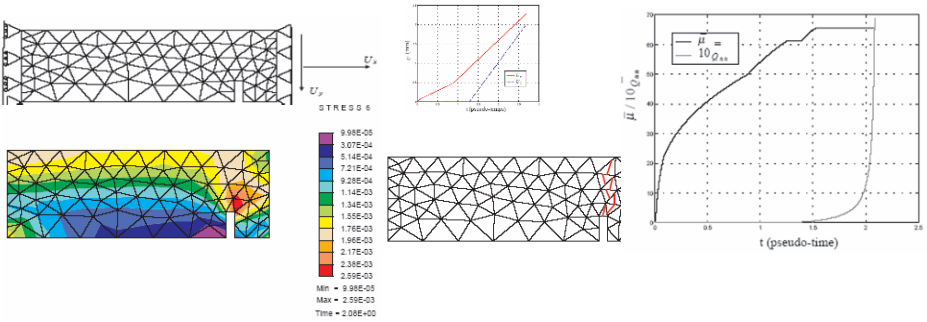

Figure 7. Micro and macro cracks for notched specimen under tensile and shear loading: loading and boundary conditions, contours of micro cracks, orientation of macro cracks, and time evolution of both damage mechanisms

In a recent work (see Ibrahimbegovic et al., 2009) we have developed the predictive model for cracking of reinforced concrete, which integrates the described concrete model for micro and macro cracks representation, along with the bond-slip model for concrete-steel interface (see Dominguez et al., 2005) accounting for frictional sliding and confinement and the standard plasticity model for steel bars including both hardening and softening that can represent different stages of failure mechanism (see Ibrahimbegovic and Brancherie, 2003). The original feature of this model for reinforced concrete concerns the X-FEM based description of the kinematics of the bond-slip that fits within the standard computer program architecture (see Fig. 8):

$$\mathrm{u}(\mathrm{x})|_{\Omega^e} = \sum_{i=1}^{4} N_i(\mathrm{x})(\mathrm{d}_i^c + \sum_{j=1}^{2} M_j(x)\alpha_j) \tag{11}$$

where N_i are standard shape functions of the chosen isoparametric element, d_i^c are concrete nodal displacements, M_j is the corresponding function introducing the global representation of bond-slip along the complete steel bar and , α_j is the nodal value of slip variable. The steel bar nodal displacement is obtained as the sum of the concrete displacement and the nodal value of bond-slip, $d_i^s = d_i^c + \alpha_i$.

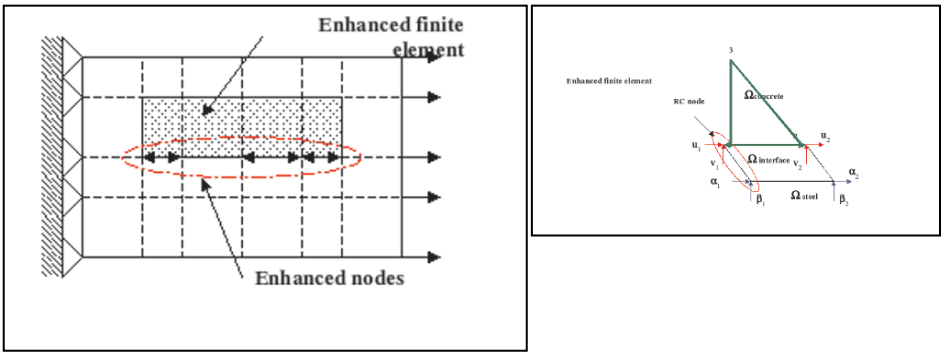

Figure 8. Extended finite element representation of reinforced concrete kinematics

The weak form of equilibrium equations associated with concrete displacements can be written:

$$
\begin{aligned}
&\mathbf{r}^{cs} := \mathop{\mathbb{A}}_{e=1}^{n_{el}} \mathbf{f}^{c,int,e}(\mathbf{d}^c_{n+1}) + \mathop{\mathbb{A}}_{e=1}^{n^{bs}_{el}} \mathbf{f}^{s,int,e}(\mathbf{d}^c_{n+1}, \boldsymbol{\alpha}_n) - \mathbf{f}^{ext}_{n+1} = 0 \; ; \\
&\mathbf{f}^{c,int,e}_i(\mathbf{d}^c_{n+1}) = \int_{\Omega^e} (\nabla^s N_i)^T \bar{\boldsymbol{\sigma}}^c_{n+1}(\mathbf{d}^c_{n+1}) dV \; ; \\
&\mathbf{f}^{s,int,e}_j(\mathbf{d}^c_{n+1}, \boldsymbol{\alpha}_n) = \int_{\Gamma^e_{bs}} (\tfrac{dM_j}{dx})^T \sigma^s_{n+1}(\mathbf{d}^c_{n+1}, \boldsymbol{\alpha}_n) dA \; ; \\
&\mathbf{f}^{ext,e}_{i,n+1} = \int_{\Omega^e} \mathbf{N}^T_i \mathbf{b} dV
\end{aligned}
\tag{12}
$$

where σ^c and σ^s are concrete and steel stress computed from the corresponding constitutive equations for the fixed value of bond slip. The remaining set equilibrium equations are associated only with the slip variation along a particular reinforcement bar:

$$
\begin{aligned}
&\mathbf{r}^{bss} := \mathop{\mathbb{A}}_{e=1}^{n^{bs}_{el}} [\mathbf{f}^{s,int,e}(\mathbf{d}^c_{n+1}, \boldsymbol{\alpha}_{n+1}) + \mathbf{f}^{bs,int,e}(\boldsymbol{\alpha}_{n+1})] = 0 \; ; \\
&\mathbf{f}^{s,int,e}_j(\mathbf{d}^c_{n+1}, \boldsymbol{\alpha}_{n+1}) = \int_{\Gamma^e_{bs}} (\tfrac{dM_j}{dx})^T \sigma^s_{n+1}(\mathbf{d}^c_{n+1}, \boldsymbol{\alpha}_n) dA \\
&\mathbf{f}^{bs,int,e}_j(\boldsymbol{\alpha}_{n+1}) = \int_{\Gamma^e_{bs}} \mathbf{B}^{bs,T} \boldsymbol{\sigma}^{bs}_{n+1}(\boldsymbol{\alpha}_{n+1}) dA
\end{aligned}
\tag{13}
$$

where σ^{bs} is the bond-slip stress. The operator split computational procedure is proposed for computing the response of this kind of reinforced concrete model can be summarized as follows:

-for $n = 0, 1, 2 \ldots$
-Given: $\mathbf{d}_n^c$, $\boldsymbol{\alpha}_n$, internal variables at t_n
-Find: $\mathbf{d}_{n+1}^c$, $\boldsymbol{\alpha}_{n+1}$, internal variables at t_{n+1}
-Iterate: $(i) = 1, 2 \ldots$
-Iterate: $(j) = 1, 2 \ldots$
compute internal variable evolution for given $\mathbf{d}_{n+1}^{c,(i)}$, $\boldsymbol{\alpha}_{n+1}^{(j)}$

$$\frac{\partial \mathbf{r}^{sbs,(i)}}{\partial \boldsymbol{\alpha}_{n+1}} (\boldsymbol{\alpha}_{n+1}^{(j+1)} - \boldsymbol{\alpha}_n^{(j+1)}) = -\mathbf{r}^{sbs}(\mathbf{d}_{n+1}^{c,(i)}, \boldsymbol{\alpha}_{n+1}^{(j)}) \; ;$$

-Test convergence locally
IF $\| \mathbf{r}^{sbs}(\mathbf{d}_{n+1}^{c,(i)}, \boldsymbol{\alpha}_{n+1}^{(j)}) \| > tol$ NEXT (j)
ELSE $\| \mathbf{r}^{sbs}(\mathbf{d}_{n+1}^{c,(i)}, \boldsymbol{\alpha}_{n+1}^{(j)}) \| < tol \Rightarrow \boldsymbol{\alpha}_{n+1}^{(i+1)} = \boldsymbol{\alpha}_{n+1}^{(j+1)}$ NEXT (i)

$$\left[\frac{\partial \mathbf{r}^{cs}}{\mathbf{d}_{n+1}^{c,(i)}} - \frac{\partial \mathbf{r}^{cs}}{\boldsymbol{\alpha}_{n+1}^{(i)}} \left(\frac{\partial \mathbf{r}^{sbs}}{\boldsymbol{\alpha}_{n+1}^{(i)}}\right)^{-1} \frac{\partial \mathbf{r}^{sbs}}{\mathbf{d}_{n+1}^{(i)}}\right] (\mathbf{d}_{n+1}^{c,(i+1)} - \mathbf{d}_{n+1}^{c,(i)}) = -\mathbf{r}_{n+1}^{cs,(i)}$$

-Test convergence globally
IF $\| \mathbf{r}^{cs}(\mathbf{d}_{n+1}^{c,(i+1)}, \boldsymbol{\alpha}_{n+1}^{(i+1)}) \| > tol$ NEXT (i)
ELSE $\| \mathbf{r}^{cs}(\mathbf{d}_{n+1}^{c,(i+1)}, \boldsymbol{\alpha}_{n+1}^{(i+1)}) \| < tol \Rightarrow \boldsymbol{\alpha}_n \longleftarrow \boldsymbol{\alpha}_{n+1}^{(i+1)}, \mathbf{d}_n \longleftarrow \mathbf{d}_{n+1}^{c,(i+1)}$

(14)

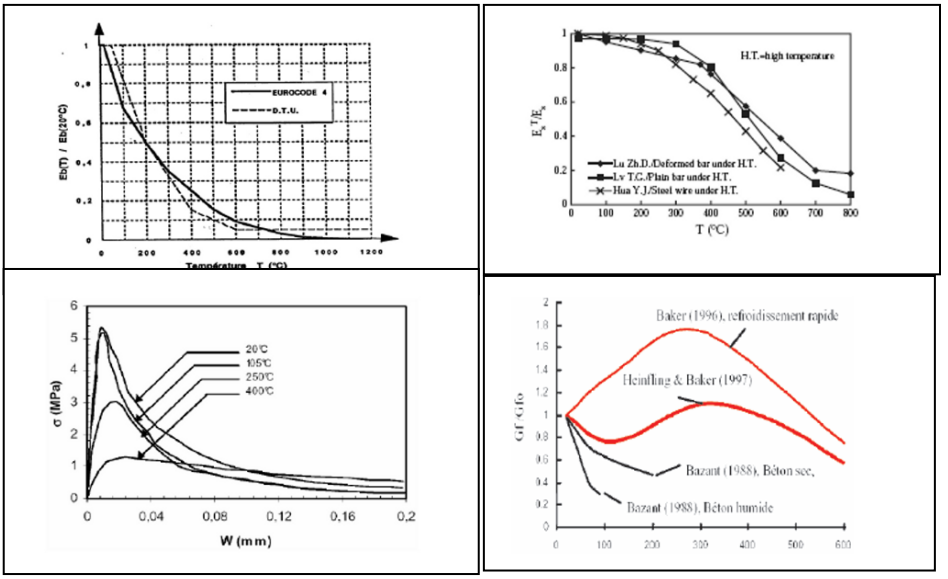

Figure 9. Temperature dependence of concrete and steel material properties showing a drop in Young's modulus values with temperature increase and change in elastic limit and in fracture energy as a function of temperature

The proposed procedure can be placed within the framework of incremental-iterative analysis with no need to change the standard computer program architecture.

When exposed to high temperatures, the material properties of steel and concrete should be modified accordingly. We can see in Fig. 9 that Young's modulus of concrete and steel drop significantly with temperature increase and so does their limits of elasticity (fracture and yield stress, respectively).

This temperature dependence of material properties is taken into account by modifying the corresponding fracture criteria for steel (see Ibrahimbegovic and Chorfi, 2002), bond-slip and concrete. The latter leads to modified form of failure criteria for micro-cracks and macro-cracks, which can be written in terms of the anisotropic damage model:

$$\begin{aligned}
&\bar{\phi}^c(\sigma,\bar{q},T) = \sqrt{\sigma\cdot D^e(T)\sigma} - \tfrac{1}{\sqrt{E(T)}}(\bar{\sigma}_f(T)-\bar{q}) \le 0\\
&\bar{\bar{\phi}}^c_n(\sigma,\bar{\bar{q}},T) = t_\Gamma\cdot n - (\bar{\bar{\sigma}}_f(T)-\bar{\bar{q}}(T)) \le 0\\
&\bar{\bar{\phi}}^c_s(\sigma,\bar{\bar{q}},T) = t_\Gamma\cdot m - (\bar{\bar{\sigma}}_s(T)-\tfrac{\bar{\bar{\sigma}}_s(T)}{\bar{\bar{\sigma}}_f(T)}.\bar{\bar{q}}(T)) \le 0
\end{aligned} \qquad (15)$$

where $D^e(T)$ is the temperature dependent damage compliance produced by micro-cracks in concrete, σ_f is elasticity limit indicating the initiation of micro-cracks, t_Γ is the driving traction at the macro-crack and σ_f and σ_s are the limits to macro-crack activation in mode I and mode II; see Brancherie and Ibrahimbegovic (2009) or Kucerova et al. (2009), for more details about the mechanical form of this model. The computational procedure that accounts for thermomechanical coupling is equivalent to the one developed previously for masonry structures (see Ibrahimbegovic et al., 2005; Colliat et al., 2005; Kassiotis et al., 2009).

We close this section by presenting the results of a couple of numerical simulations for computing the crack spacing and opening in reinforced concrete structures. The current practice of evaluating fire resistance of RC beams is based on standard fire test, in which the beam is exposed to a standard fire such as ISO 834. While standard fire resistance tests are useful benchmarks to establish the performance of RC elements under standard fire condition, they should not be relied upon to determine the survival time of RC elements under realistic fire scenarios, since they can often define less severe heating environments than those encountered in real fires. For example, we illustrate in Fig. 10 the temperature and flux time-evolutions for some realistic scenarios, derived from experimental data used for infrastructure in nuclear industry. It is important to observe in each of those scenarios a decay phase, which can also play an important role in defining the final damage of RC elements. Namely, the cross section enters a cooling phase, in which either the reinforcing steel recovers

parts of its strength and stiffness, and thus the fire resistance increase, or in the opposite produces the cracking upon unloading.

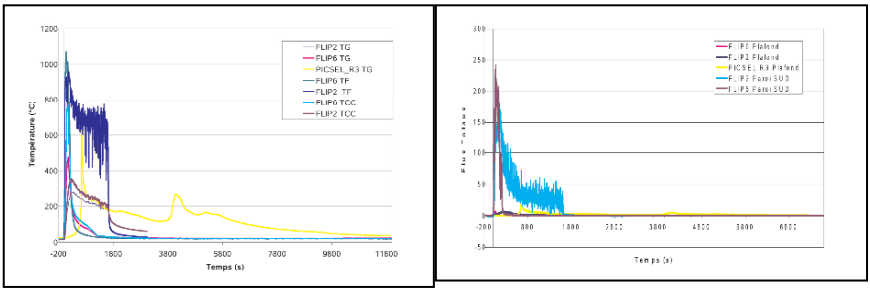

Figure 10. Fire-scenario for nuclear installation in terms of temperature and flux variations

We start with a simple example of plane concrete beam heated on one side only in order to reproduce the corresponding fire-induced conditions with temperature gradient through the thickness. To that end, a simply supported concrete slab (with dimensions: 2,350 × 2,350 × 300 mm) is heated using the critical fire-scenario for nuclear installation (see Fig. 11); applying this kind of loading.

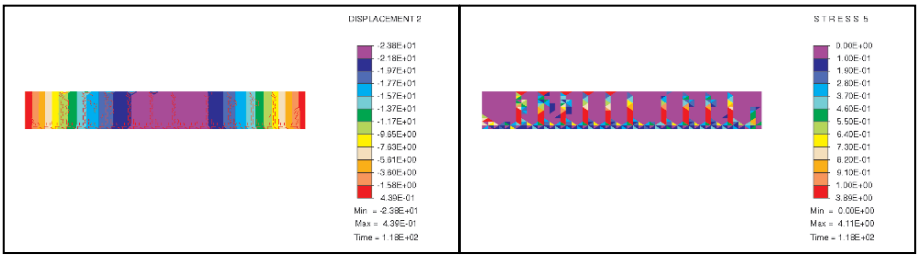

Figure 11. Crack spacing and opening of plain concrete under temperature gradient produced by heating of one side

This scenario characterizes fires were very high temperatures are reached in few seconds. Due to this severe scenario, high thermal gradient is located in a thin layer at the bottom of the slab. This loading generates compressive stresses at the bottom with subsequent traction stresses in the surface layer. It is interesting to note that we can indeed reproduce the mechanism of spalling, with the first cracks appearing in the horizontal direction. Namely, by connecting these cracks, we would finally obtain a part of the surface concrete layer to detach from the rest of the structure; this corroborates the mechanical theory of spalling induced

by steep temperature variation. The further increase in temperature leads to dominant vertical direction of crack propagation. Computed crack opening, in the range of 1–4 mm, can be considered critical in some applications in that is sufficient to allow nuclear waste to dissipate. The crack spacing remains uniform and it is equivalent to deformation mode corresponding to pure bending; this kind of result is the only consequence of homogeneous temperature field imposed on the bottom. It is important to realize that the result on crack spacing can change for a particular fire scenario with the concentrated fire source producing a heterogeneous temperature field.

The second example considers the fire-induced cracking in a reinforced concrete beam, which allows showing the positive influence of reinforcement in preventing or limiting the spalling phenomena. The reinforced concrete slab is loaded with the same critical thermal loading shown in Fig. 12, and has the same dimension as in the previous example. The main difference concerns the present of steel reinforcement with bars of 16 mm of diameter at each 10 *cm*, with a concrete cover of 30 *mm*.

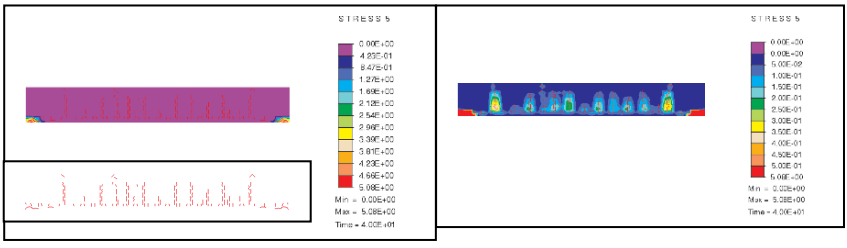

Figure 12. Crack spacing and opening of reinforced concrete under temperature gradient produced by heating of one side

In comparison with the previous case of plain concrete, the crack pattern seems quite different, which confirms that the reinforcement plays an important role. Namely, we observe fewer vertical cracks with smaller width; moreover, there is no horizontal cracks which connect and thus no spalling is observed in this case. Others numerical simulations and parametric studies are performed in order to observe the resulting crack patterns, and the conclusion can be stated as follows:

(i) Increasing the reinforcement ratio reduces the crack width.
(ii) Rising the temperature for the case when the concrete and steel don't have the same expansion coefficient, cracks width can grow slower or faster; more precisely, if steel has small coefficient of expansion relative to concrete, this produces compression in the concrete under temperature increase and hence reduces crack width.

(iii) Formation of cracks continues with the increase in ΔT until a so-called stabilized crack pattern is developed, where no further cracks can form. Hence, the distance between any two cracks cannot be smaller than a certain value called the crack spacing s.
(iv) Temperature gradient corresponding to the stabilized crack pattern is equal to $\Delta T\ s$. Further increase of ΔT beyond $\Delta T\ s$ causes widening of the existing cracks.

4. Conclusions

In this works we have briefly addressed the class of problems of damage assessment of structures and infrastructure exposed to fires. The review of a number of historical case studies show that the extreme loading conditions brought by fire exposure and resulting consequences both in peace and war times. We concluded that since the loading conditions cannot be controlled, one can put the effort in increasing the fire-resistance of modern construction materials and thus reducing the fire-induced damage. The precise thermal loading control can only be achieved in fire-resistance testing, by using additional numerical modeling as shown in this work. The tests of this kind are likely to play an important role in understanding behavior of chosen construction materials and structures and in improving their fire-resistance characteristics. A more detailed study we presented for frequently used construction material of reinforced concrete illustrates well what kind of refined models are needed in order to obtain the full understanding of complex thermomechanical failure phenomena for reinforced concrete structures and infrastructure exposed to fire. Namely, not only do we have to account for thermo-hydro-mechanical coupling at the level of material, but also for more detailed information on crack spacing and opening at the level of structure. Another important advantage of the presented model for cracks prediction in reinforced concrete is to fit within the standard computer code architecture.

Acknowledgements: this work was supported by the French Ministry of Research (funding for AB, LD), Alexander von Humboldt Research Award (to AI) and Slovenian Research Agency Award (to AI). This support is gratefully acknowledged.

References

ASTM 119-81 Standard Methods of Fire of Building Construction and Material, National Bureau of Standards, ANSI Fire Protection Group and American Society for Testing and Materials, Philadelphia, PA, 1981

Baum H.R., et. al., Gravity-current transport in buildings fires. International Conference on Fire Research and Engineering, Orlando, FL, 1995

Bazant Z.P., M.F. Kaplan, Concrete at high temperature: Material properties and mathematical modeling, Longman Harlow – Addison Wesley, 1996

Beard A., D. Drysdale, P. Holborn, S. Bishop, Configuration factor for radiation in a tunnel as partial cylinder. Fire Technology, 29, 391–402, 1993

Bendelius A.G., Tunnel fire and life safety within the world road association PIARC. The 28th ITA General Assembly, Sydney, Australia, 2002

Brancherie D., A. Ibrahimbegovic, Novel anisotropic continuum-discrete damage model capable of representing localized failure. Part I: theoretical formulation and numerical implementation. International Journal of Engineering Computations, 26, 100–127, 2009

Briollay H., P. Chasse, Validating and Optimizing 2D and 3D Computer Simulations for the Offenegg Tunnel Fire Test, Centre d´Etudes des Tunnels, Bron Cedex, France, 1994

Britter R.E., M.K.-A. Neophytou, A simple model for the movement of fire smoke in a confined tunnel. Pure and Applied Geophysics, 162, 1941, 2005

Britter R.E., P.J. Woodburn, CFD-simulations of a tunnel fire – part one. Fire Safety Journal, 26, 35, 1996

Brunello P., B.A. Schrefler, D. Gawin, C.E. Majorana, F. Pesavento, Concrete at high temperature with application to tunnel fire. Computational Mechanics, 29(1), 43, 2002

Chasse P., Sensitivity study of different modelling techniques for the computer simulation of tunnel fire. The 1st CFDS International User Conference, Oxford, UK, 1993

Chow W.K., H.T. Kot, hotel fires in Hong Kong. International Journal of Hospitality Management, 8, 271, 1989

Colliat J.B., A. Ibrahimbegovic, L. Davenne, Saint-Venant multi-surface plasticity model in strain space and in stress resultants. International Journal of Engineering Computations, 22, 536–557, 2005

Dominguez N., D. Brancherie, L. Davenne, A. Ibrahimbegovic, Prediction of crack pattern distribution in reinforced concrete by coupling a strong discontinuity model of concrete cracking and a bond-slip of reinforcement model. International Journal of Engineering Computations, 22, 558–582, 2005

Edwards J.C., C.C. Hwang, The critical ventilation velocity in tunnel fires – a computer simulation. Fire Safety Journal, 40(3), 213–244, 2005

Fay J.A., Spills and fires from LNG and oil tankers in Boston harbour. MIT, Cambridge, MA, 2003

Ferziger H., M. Peric, Computational methods for fluid mechanics. Berlin: Springer, p. 423, 2001

Gabay D., Fire safety: a short history in the Paris-subway. The 28th ITA General Assembly, Sydney, Australia, 2002

Gao P.Z., S.L. Liu, W.K. Chow, N.K. Fong, Large eddy simulations for studying tunnel smoke ventilation. Tunneling and Underground Space Technology, 19(6), 577, 2004

Gawin D., D. Pesavento, B.A. Schrefler, Modeling of deformations of high strength concrete at elevated temperatures, Materials and Structures, 27, 218–236, 2004

Holmstedt G., S. Bengston, H. Tuovinen, Sensitivity calculations of tunnel fires using CFD. Fire Safety Journal, 1, 99, 1996

Ibrahimbegovic A., Nonlinear solid mechanics: Theoretical formulations and finite element solution methods. Berlin: Springer, pp. 1–620, 2009

Ibrahimbegovic A., D. Brancherie, Combined hardening and softening constitutive model for plasticity: precursor to shear slip line failure. Computational Mechanics, 31, 88–100, 2003

Ibrahimbegovic A., L. Chorfi, Covariant principal axis formulation of associated coupled thermo-plasticity at finite strains and its numerical implementation, International Journal of Solids and Structures, 39, 499–528, 2002

Ibrahimbegovic A., J.B. Colliat, L. Davenne, Thermomechanical coupling in folded plates and non-smooth shells. Computer Methods in Applied Mechanics and Engineering, 194, 2686–2707, 2005

Ibrahimbegovic A., G. Herve, P. Villon, Nonlinear impact dynamics and field transfer suitable for parametric design studies, International Journal of Engineering Computations, 26, 185–204, 2009

Jongen T., T.B. Gatski, Nonlinear eddy viscosity and algebraic stress models for solving complex turbulent flows. Progress in Aerospace Sciences, 36, 655, 2000

Kassiotis C., J.B. Colliat, A. Ibrahimbegovic, H. Matthies, Multiscale in time and stability analysis of operator split solution procedure applied to thermomechanical problems. International Journal of Engineering Computations, 26, 205–223, 2009

Kucerova A., D. Brancherie, A. Ibrahimbegovic, J. Zeman, Z. Bittnar, Novel anisotropic continuum-discrete damage model capable of representing localized failure of massive structures. Part II: identification from tests under heterogeneous stress field. International Journal of Engineering Computations, 26, 128–144, 2009

Kumar S., G. Cox, Mathematical modelling of fires in tunnels. The 5th International Symposium on the Aerodynamics and Ventilation of Vehicle-Tunnels, Lyle, France, 1985

Kumar S., G. Cox, Mathematical modelling of fires in tunnels – Validation of JASMINE, Transport and Research Laboratory: Crowthorn, 1986

Kumar S., G. Cox, Radiation and surface roughness effects in the numerical modelling of enclosure fires. Fires Safety Science – The 2nd International Conference, Paris, France, 1988

Kunsch J.P., Simple model for control of fire gases in a ventilated tunnel. Fire Safety Journal, 37, 67, 2002

Leitner A., The fire catastrophe in the Tauern-tunnel. Tunneling and Underground Space Technology, 16(3), 217, 2001

Leupi C., Numerical modeling of cohesive sediment transport and bed morphology in estuaries, in La faculte sciences et techniques de l'íngenieur, EPFL, Lausanne, 2005

Liu S.L., P.Z. Gao, W.K. Chow, N.K. Fong, Large eddy simulations for studying tunnel smoke ventilation. Tunneling and Underground Space Technology, 19, 577, 2004

Magnussen B.F., B.H. Hjertager, On mathematical modelling of turbulent combustion with special emphasis on soot formation and combustion. The 16th International Symposium on Combustion, Pittsburgh, 1976

Malin M.R., N.C. Markatos, Mathematical modelling of buoyancy-induced smoke flow in enclosures. International Journal of Heat Mass Transfer, 25, 63, 1982

McGrattan K.B., Numerical Simulation of the Howard Street Tunnel Fire, NIST: Gaithersburg, 2002

Miles D., S. Kumar, R.D. Andrews, Validation of a CFD model for fires in the memorial tunnel. First International Conference on Tunnel FIres, Lyon, France, 1999

Miles D., S. Kumar, Computer modelling to assess the benefits of road tunnel fire safety measures. The InFlam, Edinburgh, 2004

Rojtman A., Prtotiv pozarnov normirovanie v stroitelstve. Stojizdat, Moscow, 1985

Sanmiguel-Rojas E. et al., Numerical model and validation experiments of atrium enclosure fire in a new fire test facility. Building and Environment, 43, 1912–1928, 2007

Sawley M., A. Drotz, SOCATOP, Lausanne, Switzerland, 2003

Schrefler B.A., F. Pesavento, L. Sanavia, D. Gawin, Multi-physics problems in thermo-hydro-mechanical analysis of partially saturated geomaterials. In Ibrahimbegovic A., B. Brank (eds.), Multi-physics and multi-scale computer models in nonlinear analysis and optimal design of engineering structures under extreme conditions, IOS Press, Amsterdam (ISBN 1-58803-479-0), pp. 1–407, 2005

Simulation of fires in tunnels under construction, SINTEF: Trondheim, Norway, 2005

Tan G.L., Fire fighting in tunnels. Tunneling and Underground Space Technology, 17(2), 179, 2002

Tuovinen H., Validation of ceiling jet flows in a large corridor with vents using the CFD code JASMINE. Fire Technology, 32, 34–45, 1994

Ulm F.J., O. Coussy, Z.P. Bazant, The Chunnel fire: Part I: Chemoplastic softening in rapidly heated concrete. ASCE Journal of Engineering in Mechanics, 125, 378–385, 1999

Versteeg H.K., W. Malalasekera, An introduction to computational fluid dynamics, Longman Group Ltd.: London, 1995

Vidmar P., S. Petelin, Analysis of the effect of an external fire on the safety operation of an powerplant. Fire Safety Journal, 41, 486, 2006

Vladimirova N., Model flames in the Boussinesq limit, ASC/Flash Center, Dept. of Astronomy and Astrophysics, The University of Chicago, Chicago, IL, 2006

Wighus R., Fire at sea-surface, SINTEF: Spitzbergen, Norway, 1994

Zhang W., et al., Turbulence statistics in a fire room model by large eddy simulation. Fire Safety Journal, 37, 721, 2002